DOI: 10.1002/ejic.200900112

Thermodynamic and Structural Investigations on the Complexation Process of Dioxo Macrocyclic Ligands: Towards Neutral Copper Complexes at Physiological pH

Isabelle Déchamps-Olivier,[a] Cyril Cadiou,[a] Dominique Harakat,[b] Thierry Roisnel,[c] Françoise Chuburu,*[a] Jana Hodacova,[d] and Simona Koscova[e]

Keywords: Macrocyclic ligands / Thermodynamics / UV/Vis spectroscopy / Copper

Two dioxotetraza macrocycles 9,12,16,19-tetraazatricyclo-[19.4.0.0^{2,7}]pentacosa-1(21),2,4,6,22,24-hexaene-8,20-dione (**L^1**) and 9,13,16,20-tetraazatricyclo[20.4.0.0^{2,7}]hexacosa-1(22),2,4,6,23,25-hexaene-8,21-dione (**L^2**) and two bis(dioxotetraaza) macrocycles 7,10,14,17,25,28,32,35-octaazatetracyclo[17.17.2.0^{5,37}.0^{23,38}]octatriaconta-1,3,5(37),19,21,23(38)-hexaene-6,18,24,36-tetrone (**L^3**) and 7,11,14,18,26,30,33,37-octaazatetracyclo[18.18.2.0^{5,39}.0^{24,40}]tetraconta-1,3,5(39),20,22,24(40)-hexaene-6,19,25,38-tetrone (**L^4**) were prepared. Their protonation constants and the overall complexation constants of their copper(II) complexes were determined by potentiometry at 25 °C (I = 1, KNO_3). In aqueous solution, the complexation sequence was elucidated for each ligand by means of UV/Vis and EPR spectroscopy. According to the ligand structure, two complexation mechanisms can be characterized. For ligand **L^1**, a neutral complex [Cu**L^1**H$_{-2}$] is readily obtained in one step at pH ≈ 5, and it is the sole species above pH 7. Its structure was confirmed by X-ray analysis. For ligands **L^2** and **L^4**, the neutral complexes [Cu**L^2**H$_{-2}$] and [Cu$_2$**L^4**H$_{-4}$] were formed by successive deprotonation of [Cu**L^2**]$^{2+}$ and [Cu$_2$**L^4**]$^{4+}$, respectively.

Introduction

The replacement of amine by amide groups in macrocyclic polyamines yields a class of ligands, which have been studied in detail since the first synthesis of 1,4,8,11-tetraazacyclotetradecane-5,7-dione by Tabushi et al.[1] These diamino–diamido ligands exhibit unique features: in slightly acidic solution, they are poor ligands (in their LH_2 form), but on increasing the pH they are powerful binders. The first complexation studies have shown that at sufficiently high pH and in the presence of appropriate divalent metal ions, the two amido protons are released to give the ligands a diamino–diimido doubly negative four-donor set, capable of forming very stable neutral complexes.[2–4] Moreover, these ligands are selective as only Co^{2+}, Ni^{2+} and Cu^{2+}, among the first row transition-metal cations, can promote the deprotonation of the amido groups to form neutral [ML] complexes.[5] The resulting complexes are interesting in many respects, such as building blocks for polymetallic systems[6] useful in molecular magnetism.[7] In addition, the diamino–diamido ligands can be functionalized by appending coordinating groups to the primary amines without altering their coordinative features. In the presence of Ni^{2+} or Cu^{2+}, these smart ligands behave as pH-driven molecular machines that are able to translocate metal cations.[8] In certain cases, they are even capable of acting as anion receptors that can be open and closed on command.[9]

Recently, dioxotetraza macrocyclic ligands having two diamino and two diamido functions in a tetraaza macrocyclic framework have been developed for medical applications,[3,4,10,11] in particular, to deliver metal radionuclides, such as copper radionuclides.[12,13] These chelates provide an excellent binding environment for Cu^{2+} ions as they combine their rapid metallation ability, small size and aqueous solubility with their resistance to exchange of Cu^{2+} in vivo.[14] An understanding of the in vivo chemistry of the radiocopper chelates has furthermore shown that the formal charge of the complexes has a great influence on their clearance from the body. While positively charged complexes show high retention in the kidneys and the liver 24 h post injection, the negatively charged or neutral complexes

[a] ICMR CNRS UMR 6229, Groupe Chimie de Coordination, Université de Reims Champagne-Ardenne, BP 1039, 51687 Reims Cedex 2, France
E-mail: francoise.chuburu@univ-reims.fr
[b] ICMR CNRS UMR 6229, Service commun d′analyses, Université de Reims Champagne-Ardenne, BP 1039, 51687 Reims Cedex 2, France
[c] UMR CNRS 6511, Institut de Chimie de Rennes, CS 74205, 35042 Rennes Cedex, France
[d] Department of Organic Chemistry, Institute of Chemical Technology, Technická 5, 166 28 Prague 6, Czech Republic
[e] Institute of Organic Chemistry and Biochemistry, Academy of Sciences of the Czech Republic, Flemingovo nam. 2, 166 10 Prague 6, Czech Republic

Supporting information for this article is available on the WWW under http://dx.doi.org/10.1002/ejic.200900112.

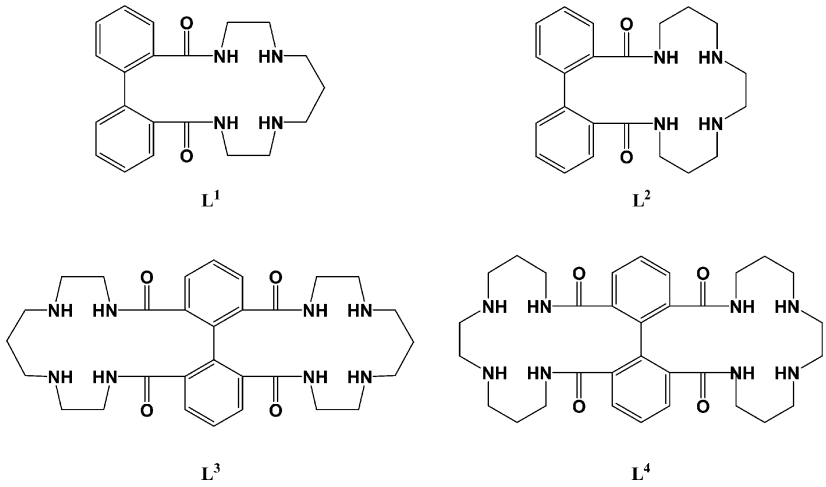

Scheme 1.

have a lower liver uptake and a rapid and efficient clearance through the kidneys.[10] In this context, the potential usefulness of the dioxotetraaza macrocycles as neutral chelates for copper is evident. In this work, we have undertaken the synthesis of four new dioxo macrocyclic ligands **L¹**–**L⁴** (Scheme 1) in order to evaluate their binding ability towards copper(II). Hence, a thermodynamic investigation of the complexation reaction was carried out. The corresponding complexes were further characterized by electronic, EPR spectroscopy and, in the case of ligands with a single cavity (**L¹**, **L²**), by X-ray diffraction.

Results and Discussion

Acid–Base Behaviour

The acid–base behaviour of the four ligands **L¹**–**L⁴** was investigated through potentiometric titrations at 25 ± 0.1 °C by adding KOH (0.1 mol L^{-1}). The ionic strength was adjusted to 1 with KNO_3, the presence of nitric acid allowing the protonation of the ligands.

The titrations of solutions of **L¹**–**L⁴** gave rise to neutralisation curves with three inflexion points. In all cases, the first inflexion point corresponds to the neutralisation of the strong acid in excess (Figure S1). For **L¹** and **L²**, the two following equivalent points correspond to the stepwise deprotonation of the LH_2^{2+} entities, since in acidic medium both ligands are doubly protonated. For **L³** and **L⁴**, in acidic medium both ligands are four-fold protonated, which implies that the two following equivalent points correspond to the stepwise deprotonation of the LH_4^{4+} species. The mathematical treatment of these data with PROTAF software[15] allowed the determination of log K_{01h} values for these ligands and those of ligands **L⁵**–**L⁸** (Table 1 and Scheme 2).

For **L¹** and **L²**, two protonation constants have been determined (Table 1). These values ($\log K_{011}$ = 9.19 and $\log K_{012}$ = 7.00 for **L¹** and $\log K_{011}$ = 9.41 and $\log K_{012}$ = 6.27 for **L²**) are similar to the values determined for **L⁵**.[16] They correspond to the protonation of the secondary amine functions located at the vicinity of amide functions in a macrocyclic framework. From **L²** to **L¹**, the first $\log K_{011}$ value decreases from 9.41 to 9.19. This indicates that the ring size of **L²** is much more adapted than that of **L¹** and stabilizes the first proton added, by hydrogen bonding. Furthermore, large values of $\Delta\log K_{12} = \log K_{011} - \log K_{012}$ are observed for **L¹** and **L²** (2.19 and 3.14, respectively). This can be interpreted in terms of the electrostatic repulsive effect between the two protonated adjacent amino nitrogen atoms. Consequently in **L²**, where the two secondary amino nitrogen atoms are separated by an ethylene bridge, the electrostatic repulsion is higher, which enhances the acidity of the second proton added.

The **L¹** and **L²** protonation constants can be compared to the two first protonation constants of their reduced analogues **L⁶** and **L⁷** [($\log K_{011}$ = 11.01, $\log K_{012}$ = 10.88) and ($\log K_{011}$ = 9.70, $\log K_{012}$ = 8.73), respectively].[17] The acidity is in fact enhanced in **L¹** and **L²**, and it can be correlated to the spatial proximity of the electropositive end of the keto groups to the amino functions.[3,18] Finally, one should observe that the **L¹** and **L²** amide protons are not acidic enough to be deprotonated in water.

Table 1. Protonation constants for ligands **L¹**–**L⁸**.[a]

log K_{01h}	**L¹**	**L²**	**L³**	**L⁴**	**L⁵**[16]	**L⁶**[17a]	**L⁷**[17b]	**L⁸**[16]
$L + H^+ \rightleftarrows LH^+$	9.19(8)	9.41(3)	9.44(8)	9.65(2)	9.51	11.01	9.70	9.96
$LH^+ + H^+ \rightleftarrows LH_2^{2+}$	7.00(4)	6.27(4)	8.88(4)	9.11(2)	5.80	10.88	8.73	9.45
$LH_2^{2+} + H^+ \rightleftarrows LH_3^{3+}$			7.36(4)	6.47(1)		2.20	6.42	5.40
$LH_3^{3+} + H^+ \rightleftarrows LH_4^{4+}$			6.47(3)	5.91(1)		<2	4.02	4.62

[a] The numbers in parentheses refer to the estimated standard deviations for the last significant digit (95% confidence).

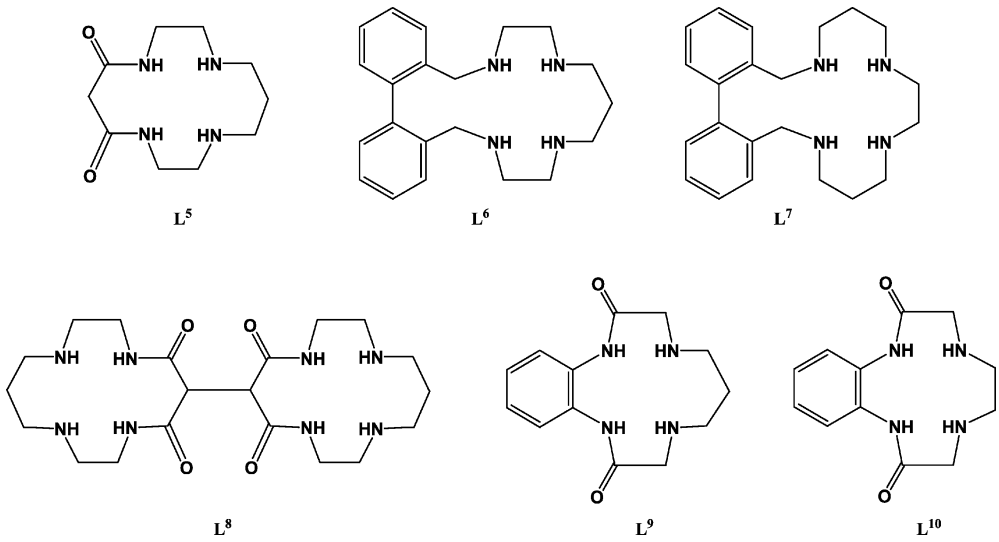

Scheme 2.

For $\mathbf{L^3}$ and $\mathbf{L^4}$, four protonation constants have been determined (Table 1). The first two should be compared with the first protonation constant of the sole cavity ($\mathbf{L^1}$ or $\mathbf{L^2}$, respectively). This similarity between the values indicates that in bismacrocyclic ligands the two first protons are added alternatively in the two cavities. These observations still hold for the third and fourth protonations. This can be easily understood in terms of minimization of electrostatic repulsion between positive charges in the protonated species.[16,19]

Thermodynamic Investigations of the Complexation Reaction of the Dioxo Macrocycles $\mathbf{L^1}$ and $\mathbf{L^2}$ with Copper

The titration of acidic solutions of $\mathbf{L^1}$ and $\mathbf{L^2}$ was undertaken in the presence of copper for several [L]/[M] ratios. The data analysis by PROTAF software[15] showed that for each ligand, the best curve fitting is obtained by assuming the formation of $[CuL]^{2+}$, $[CuLH_{-1}]^{+}$ and $[CuLH_{-2}]$ complexes. The corresponding overall formation constants are reported in Table 2. For both ligands, the two first values, $\log \beta_{110}$ and $\log \beta_{11-1}$, are similar and smaller than the one found for the ligand $\mathbf{L^5}$ ($\log \beta_{110} = 8.75$).[16] This can be correlated with the fact that in the copper complexes of $\mathbf{L^1}$ and $\mathbf{L^2}$, the macrocyclic cavity is larger than in that of $\mathbf{L^5}$, and the metal profits less from any macrocyclic effect.[8a]

Table 2. Overall formation constants for $\mathbf{L^1}$, $\mathbf{L^2}$ and $\mathbf{L^5}$.[a]

$\log \beta_{m\ell h}$	$\mathbf{L^1}$[b]	$\mathbf{L^1}$[c]	$\mathbf{L^2}$[b]	$\mathbf{L^2}$[c]	$\mathbf{L^5}$[16]
$Cu^{2+} + L \rightleftarrows [CuL]^{2+}$	6.2(1)		6.89(1)	7.04	8.75
$Cu^{2+} + L \rightleftarrows [CuLH_{-1}]^{+} + H^{+}$	–0.3(4)		–0.2(1)	0.18	
$Cu^{2+} + L \rightleftarrows [CuLH_{-2}] + 2H^{+}$	–5.25(2)	–5.30	–10.2(1)	–9.32	0.44

[a] Potentiometric titrations. [b] Spectrophotometric titrations. [c] The numbers in parentheses refer to the estimated standard deviations for the last significant digit (95% confidence).

However, for $\mathbf{L^1}$ and $\mathbf{L^2}$, the third value, $\log \beta_{11-2}$, is markedly different; the $[Cu\mathbf{L^1}H_{-2}]$ complex is more stable than $[Cu\mathbf{L^2}H_{-2}]$. This discrepancy leads to a major difference in the respective distribution diagrams of the Cu^{2+}–dioxo macrocyclic systems (molar ratio 1:1, Figure 1). For $\mathbf{L^1}$, the $[Cu\mathbf{L^1}]^{2+}$ and $[Cu\mathbf{L^1}H_{-1}]^{+}$ complexes are only minor

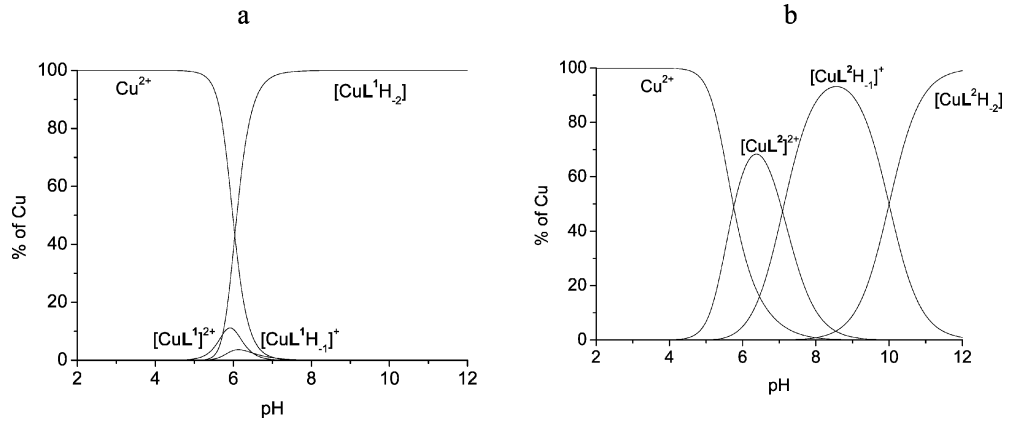

Figure 1. Species distribution diagrams for the Cu^{II} complexes with (a) $\mathbf{L^1}$ and (b) $\mathbf{L^2}$. $c_L = 2.50 \times 10^{-3}$ mol·L^{-1}, $c_M = 2.50 \times 10^{-3}$ mol L^{-1}.

species (the maximum concentration reaches 10% at pH = 6, Figure 1a), and the formation of the major species, $[Cu\mathbf{L^1}H_{-2}]$, begins at pH 5 and is complete at pH 7.

For $\mathbf{L^2}$, higher percentages of complexes with the non-deprotonated amide, $[Cu\mathbf{L^2}]^{2+}$, and the mono-deprotonated amide, $[Cu\mathbf{L^2}H_{-1}]^{+}$, were determined. Their stability is therefore increased relative to that of $[Cu\mathbf{L^1}]^{2+}$ and $[Cu\mathbf{L^1}H_{-1}]^{+}$, respectively. Consequently, the final neutral complex, $[Cu\mathbf{L^2}H_{-2}]$, is obtained at higher pH values (only above pH 11 instead of pH 7, as in the case of $[Cu\mathbf{L^1}H_{-2}]$).

In order to compare the affinity of ligands $\mathbf{L^1}$ and $\mathbf{L^2}$ for copper at physiological pH with the affinity of ligands $\mathbf{L^9}$ and $\mathbf{L^{10}}$ developed by Delgado et al.[3] for radiomedical applications, the determination of pCu ($-\log[Cu^{2+}]$) has to be undertaken. At pH 7.4, for [L] = [M] = 5×10^{-3} mol L^{-1}, the pCu values for $\mathbf{L^1}$ and $\mathbf{L^2}$ are 4.95 and 3.82, respectively, while the corresponding values for $\mathbf{L^9}$ and $\mathbf{L^{10}}$ are 9.67 and 4.09, respectively; the metal affinity of $\mathbf{L^1}$ is between those of $\mathbf{L^9}$ and $\mathbf{L^{10}}$, and $\mathbf{L^2}$ and $\mathbf{L^{10}}$ have a similar efficiency. As the size of the macrocyclic cavity is larger in $\mathbf{L^1}$ and $\mathbf{L^2}$, the macrocyclic effect is less effective than in $\mathbf{L^9}$, which results in a less efficient complexation of Cu^{2+}, as previously mentioned. Moreover, the fact that $\mathbf{L^1}$ and $\mathbf{L^2}$ are less efficient than $\mathbf{L^9}$ may also be correlated to the steric strain due to the biphenyl moiety: with this moiety, the rearrangement of the donor atoms of $\mathbf{L^1}$ and $\mathbf{L^2}$ for coordination probably requires an amount of energy that is not compensated for in the final structure of the complex.

UV/Vis and EPR Spectral Characteristics of the Copper Complexes of $\mathbf{L^1}$ and $\mathbf{L^2}$

To gain an insight into the nature of the copper coordination sphere in these complexes, the metal coordination process was monitored by UV/Vis and EPR spectroscopy. In the visible region of the electromagnetic spectrum, the copper complexes exhibit broad absorption bands associated with metal d–d transitions (Figures 2 and 3). For the {Cu–$\mathbf{L^1}$} system above pH 5, the spectrum exhibits two bands at λ_{max} = 600 and 790 nm, which do not shift to higher energy when the pH is raised (Figure 2a). This spectrum is compatible with a CuN_4 chromophore.[20] Furthermore, the profile for the absorption at λ = 600 nm vs. pH correlates well with the formation of $[Cu\mathbf{L^1}H_{-2}]$ (Figure 2b), which is in agreement with potentiometric measurements.

The EPR spectrum of a Cu–$\mathbf{L^1}$ solution at pH 10 (Figure S2), where $[Cu\mathbf{L^1}H_{-2}]$ is exclusively formed, can provide additional information about the metal environment. The spectrum exhibits four well-resolved lines, as expected for the unpaired electron density of the copper(II) nucleus. From the corresponding EPR parameters (Table 3) the $g_{\|}/A_{\|}$ ratio, which is a good indicator of the stereochemistry around the copper, as well as an empirical index of the distortion for a tetragonal geometry[21] can be calculated. For $[Cu\mathbf{L^1}H_{-2}]$, this ratio is of 134.8 cm, which indicates that the copper is held in a distorted tetrahedral geometry.

For the {Cu–$\mathbf{L^2}$} system, a blueshift of the UV/Vis signal from 825 to 540 nm is observed as the pH is raised (Figure 3a). The evolution of the λ_{max} value as a function of pH follows a sigmoidal curve with three distinct steps (Figure 3b). The curve shape is in agreement with the formation of three consecutive complexes as suggested by potentiometric measurements. In the pH range 5–7, the spectrum exhibits a broad band centred at λ_{max} = 680 nm, which corresponds to the $[Cu\mathbf{L^2}]^{2+}$ complex. For this species, one can propose that the metal is coordinated only by the ligand amine functions since the amide functions are not deprotonated at these pH values. The metal coordination sphere must then be completed by solvent molecules. In the pH range 7–10, the spectrum presents a broad band centred at λ_{max} = 600 nm, which corresponds to the $[Cu\mathbf{L^2}H_{-1}]^{+}$ complex in which the metal is coordinated by the amine functions of the ligand, by one deprotonated amide function and, probably, by one solvent molecule (Figure 4). Finally, for pH values higher than 11, a new broad band appears at 540 nm, which corresponds to the presence of $[Cu\mathbf{L^2}H_{-2}]$ in solution. The position of this band is typical of a CuN_4 chromophore with the metal atom held in a square-planar geometry.[22] This proposal is corroborated by the EPR spectrum of $[Cu\mathbf{L^2}H_{-2}]$ and by the corresponding electronic

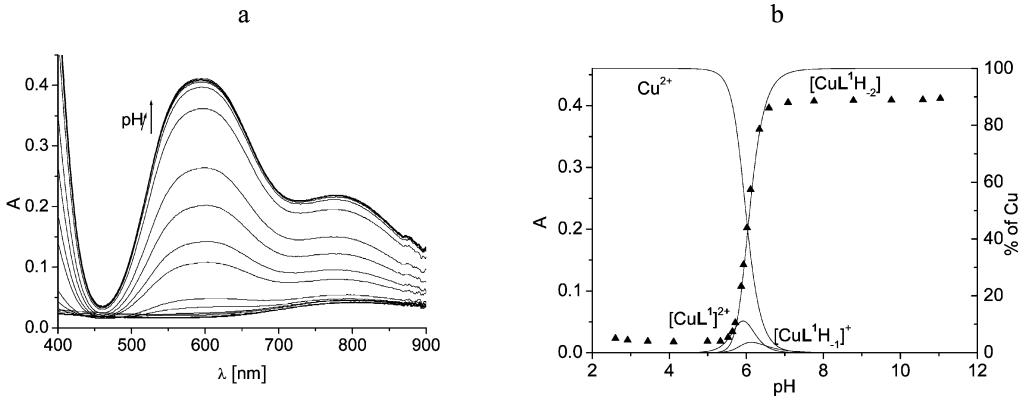

Figure 2. (a) Spectrophotometric titrations of the {Cu–$\mathbf{L^1}$} system with KOH (0.1 mol L^{-1}), $c_L = 1.65\times10^{-3}$ mol L^{-1}, $c_M = 1.25\times10^{-3}$ mol L^{-1}; (b) λ(600 nm) = f(pH).

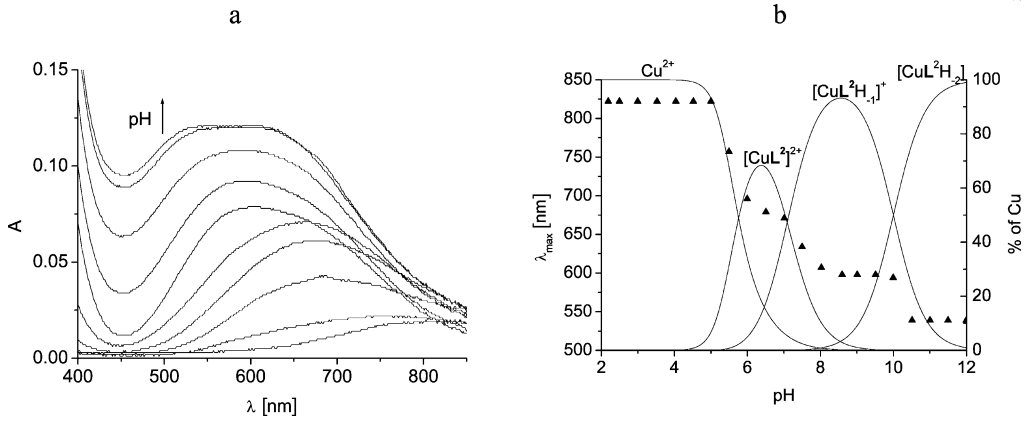

Figure 3. (a) Spectrophotometric titrations of the {Cu–**L²**} system with KOH (0.1 mol L^{-1}), $c_L = 1.65 \times 10^{-3}$ mol L^{-1}, $c_M = 1.25 \times 10^{-3}$ mol L^{-1}; (b) $\lambda_{max} = f(pH)$.

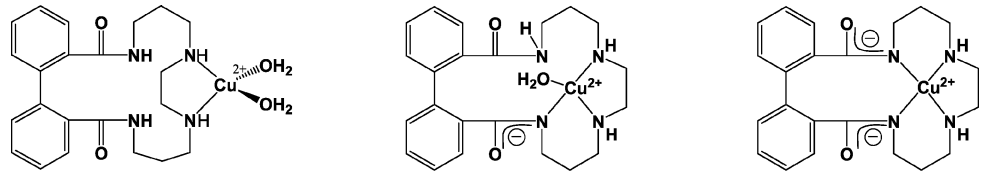

Figure 4. Suggested coordinative arrangements of the copper ion in the **L²** complexes.

Table 3. UV/Vis data for the solid state and for solution, EPR parameters in frozen solutions for the **L¹** and **L²** copper complexes.

Species	λ [nm] (ε [mol^{-1} L cm^{-1}])		$g_{//}$	$A_{//}$ (10^{-4} cm^{-1})	$g_{\perp}$
	Solid state	Solution			
[Cu**L¹**H$_{-2}$][a]		790 (88)/600 (164)	2.220	164.7	2.046
[Cu**L¹**H$_{-2}$][b]	798/601	810/600	2.207	159.4	2.044
[Cu**L²**H$_{-2}$][a]		660 (110)/540 (110)	2. 236	185.8	2.05
[Cu**L²**(OAc)$_2$][b]	680	683	2.267	170.1	2.052

[a] Spectroscopic data from solution studies – EPR conditions: water/glycerol (150 K). [b] Spectroscopic data from single crystals – EPR conditions: MeOH (150 K).

parameters (Table 3, Figure S2). For [Cu**L²**H$_{-2}$], the $g_{//}/A_{//}$ ratio of 120.3 cm is effectively consistent with a square-planar geometry that is slightly distorted around the metal ion.[21]

Structural Investigations of the Copper Complexes of L¹ and L²

Structural investigations of the copper(II) complexes of **L¹** and **L²** were carried out in the solid state in order to confirm the hypotheses formulated during the solution studies.

The syntheses of the complexes were performed in methanol by addition of Cu(OAc)$_2$. Single crystals suitable for an X-ray analysis were obtained with both ligands. They were isolated by slow diffusion of ethyl ether into a methanolic solution of the complexes. The crystal data and details of the structure determination are given in Table S1, while selected geometrical parameters are given in Table 4.

An ORTEP depiction of the copper complex obtained with **L¹** is provided in Figure 5. This complex corresponds to the formula [Cu**L¹**H$_{-2}$], where the copper ion is held in a distorted tetrahedral geometry. The metal ion is coordinated by the two amine groups of the macrocycle and the two deprotonated amido groups of the ligand. This is confirmed by the IR spectrum (KBr pellets) where a shift of the carbonyl amido vibration between the ligand (1623 cm^{-1}) and the complex (1537 cm^{-1}) is observed. The Cu–N bond lengths are in the range observed for [Cu**L⁹**H$_{-2}$].[3] The two Cu–N(imido) distances [1.967(2) and 1.974(2) Å] are shorter than the two Cu–N(amino) distances [2.022(2) Å] owing to the harder character of the donor atom. The two benzene moieties of the biphenyl subunit are twisted, and the C(a)–C(b)–C(c)–C(d) angle is 107°. Consequently, the metal ion is wrapped in the ligand framework. The UV/Vis absorption spectrum of the single crystals of [Cu**L¹**H$_{-2}$] was recorded in solid-reflectance mode and in solution in methanol (Table 3) to obtain a comparison of the structure in the solid state and in solution. With regard to the band for copper, the concordance of the solid state and the solution spectroscopic data (two λ_{max} bands at about 810 and 600 nm) implies that the copper environment in maintained on going from the solid state to solution. These bands are consistent with a tetrahedral CuN_4 chromophore.[21]

Table 4. Selected bond lengths [Å] and angles [°] for [Cu$\mathbf{L^1}$H$_{-2}$] and [Cu$\mathbf{L^2}$(OAc)$_2$], for which two molecules (mol 1 and mol 2) are present in the crystal.

[Cu$\mathbf{L^1}$H$_{-2}$]			
Cu–N(1)	1.967(2)	N(1)–Cu–N(2)	113.4(1)
Cu–N(2)	1.974(2)	N(1)–Cu–N(3)	149.0 (1)
Cu–N(3)	2.022(2)	N(2)–Cu–N(4)	150.2 (1)
Cu–N(4)	2.022(2)	N(2)–Cu–N(3)	82.8 (1)
		N(1)–Cu–N(4)	85.9(1)
		N(3)–Cu–N(4)	91.7 (1)
[Cu$\mathbf{L^2}$(OAc)$_2$]	mol 1/mol 2		mol 1/mol 2
Cu–N(1)	2.033(6)/2.034(6).	O(1)–Cu–O(2)	56.57(2)/55.80(2)
Cu–N(2)	2.066(5)/2.045(6)	O(1)–Cu–O(3)	84.87(2)/84.88(2)
Cu–O(1)	1.974(5)/1.975(6)	O(3)–Cu–O(4)	57.20(2)/56.99 (2)
Cu–O(4)	2.004(4)/2.017(5)	O(2)–Cu–O(4)	94.88(2)/96.07(2)
Cu–O(2)	2.602(4)/2.587(4)	O(1)–Cu–O(4)	91.76(2)/90.96(2)
Cu–O(3)	2.539(5)/2.513(5)	O(1)–Cu–N(1)	174.09(2)/172.38(2)
		O(2)–Cu–N(1)	118.15(2)/117.31(2)
		O(3)–Cu–N(1)	101.04(2)/102.73(2)
		O(4)–Cu–N(1)	91.38(2)/93.22(2)
		N(1)–Cu–N(2)	86.78(2)/85.18(3)
		O(1)–Cu–N(2)	90.03(3)/91.0 (2)
		O(2)–Cu–N(2)	85.56(2)/87.7(3)
		O(3)–Cu–N(2)	123.66(2)/120.03(2)
		O(4)–Cu–N(2)	178.10(2)/176.23(2)
		O(3)–Cu–O(2)	132.95 (2)/133.38(2)

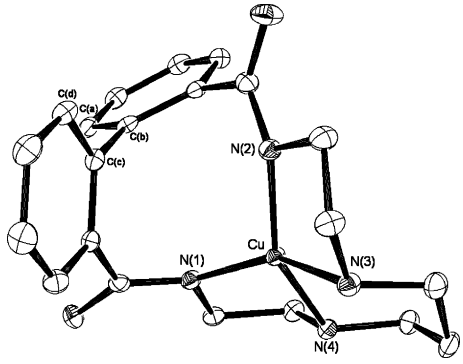

Figure 5. ORTEP diagram of [Cu$\mathbf{L^1}$H$_{-2}$].

The ORTEP depiction of the copper complex obtained with $\mathbf{L^2}$ is provided in Figure 6. Two very similar complexes are present in the crystal. Each complex corresponds to the formula [Cu$\mathbf{L^2}$(OAc)$_2$], where the copper ion is hexacoordinate. The metal ion is coordinated by the two amine functions of the ligand and by two acetate groups; each acetate ion is bound to the metal in a bidentate fashion. The Cu–N bond lengths [2.03–2.07 Å] are longer than those for [Cu$\mathbf{L^1}$H$_{-2}$], while the Cu–O bond lengths are in the range [1.97–2.61 Å]. The two benzene moieties of the biphenyl subunit are still twisted, the C(a)–C(b)–C(c)–C(d) angle (100° and 102°) is close to that measured for [Cu$\mathbf{L^1}$H$_{-2}$] (107°). The structure of [Cu$\mathbf{L^2}$(OAc)$_2$] clearly demonstrates that the two amide functions are not deprotonated and do not participate in the bonding at the metal coordination sphere. This is confirmed by IR spectroscopy, since the spectrum shows an amide vibration at 1628 cm^{-1} for the complex and 1627 cm^{-1} for the ligand. The IR spectrum of the [Cu$\mathbf{L^2}$(OAc)$_2$] complex also exhibits two vibrations at 1522 cm^{-1} and 1393 cm^{-1} in the carbonyl region that can be attributed to the ν_{as} and ν_s vibrations of the acetate groups. The difference between these two absorption frequencies (Δ = 129 cm^{-1}) can be compared to the value obtained for the noncoordinated ionic species (Δ_{ionic} = 164 cm^{-1}[23]). Since the gap Δ for [Cu$\mathbf{L^2}$(OAc)$_2$] is smaller than that for the free ion, Δ_{ionic}, a bidentate coordination mode for the acetate counterions in [Cu$\mathbf{L^2}$(OAc)$_2$] is seen.[23,24] The UV/Vis absorption spectrum of the single crystals was recorded in solid-reflectance mode and in methanol to compare the structure of [Cu$\mathbf{L^2}$(OAc)$_2$] in the solid state and in solution (Table 3). Irrespective of the conditions, the [Cu$\mathbf{L^2}$(OAc)$_2$] spectrum exhibits only one band at λ_{max} = 680 nm. This band, low in energy for a tetraaza macrocyclic complex [510 < λ < 530 nm for an N-monofunctionalized cyclam copper(II) complex],[25] can be attributed to a hexacoordinate complex (for which λ_{max} is located between 625 and 740 nm[26]). One should note that the UV/Vis data, as well as the EPR electronic parameters (Table 3) recorded for single crystals of [Cu$\mathbf{L^2}$(OAc)$_2$], strongly differ from the data recorded during the course of the solution studies for the species [Cu$\mathbf{L^2}$H$_{-2}$]. This reinforces the fact that for the {Cu –$\mathbf{L^2}$} system and according to the pH, several complexes can be observed in solution.

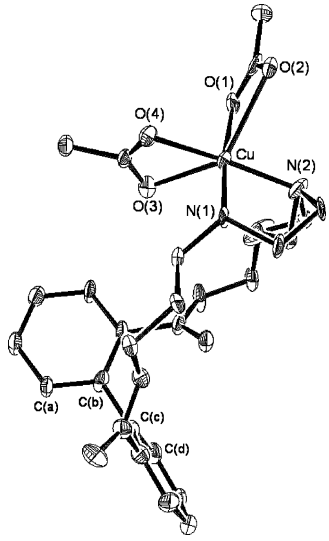

Figure 6. ORTEP diagram of [Cu$\mathbf{L^2}$(OAc)$_2$].

Complexation of Bis(dioxo) Macrocycles $\mathbf{L^3}$ and $\mathbf{L^4}$ with Copper

Titrations of acidic solutions of $\mathbf{L^3}$ and $\mathbf{L^4}$ were performed in the presence of copper for several [L]/[M] ratios.

Incorporation of a Single Cu^{II} Ion

Irrespective of the ligand $\mathbf{L^3}$ or $\mathbf{L^4}$, for [L]/[M] > 1, the best curve for the pH range 4–12 was obtained by assuming the formation of complexes having the following stoichio-

metry $[CuLH_2]^{4+}$, $[CuLH]^{3+}$, $[CuL]^{2+}$, $[CuLH_{-1}]^{+}$ and $[CuLH_{-2}]$. The ESI-MS spectra of these solutions (Figure 7, Table 5) confirms the presence of mononuclear copper complexes and ligand in excess (as proton and potassium adducts). The calculated distribution diagram is reported in Figure 8, and the corresponding overall formation constants are gathered in Table 6. In each case, the first complex formed has the formula $[CuLH_2]^{4+}$. One can propose that only one dioxo macrocyclic subunit is involved in the complexation, while the other moiety is diprotonated. Therefore, if we consider that in the species $[Cu\mathbf{L^3}H_2]^{4+}$ and $[Cu\mathbf{L^4}H_2]^{4+}$, the two dioxo macrocyclic subunits behave independently; the log β_{112} value of these two species must compare with the sum of the log β_{110} value of the Cu^{II} complexes of $\mathbf{L^1}$ and $\mathbf{L^2}$, respectively, and the protonation constants log K_{011} and log K_{012} of the $\mathbf{L^1}$ and $\mathbf{L^2}$ ligands, respectively (Tables 1 and 2). Therefore, for $\mathbf{L^1}$, the sum of these values is 22.39 log units, while the experimental value for $[Cu\mathbf{L^3}H_2]^{4+}$ is 23.05. For $\mathbf{L^2}$, the sum of these values is 22.57 log units, while the experimental value for $[Cu\mathbf{L^4}H_2]^{4+}$ is of 22.90. The good agreement between these values illustrates that, as suspected, the two dioxo macrocyclic subunits behave independently, which can be ascribed to the presence of the biphenyl spacer which forces the two subunits to be independent.[27] As the pH is increased, several deprotonated forms of the species $[Cu\mathbf{L^3}H_2]^{4+}$ and $[Cu\mathbf{L^4}H_2]^{4+}$ are calculated: in order to propose a deprotonation sequence for $[Cu\mathbf{L^3}H_2]^{4+}$ and $[Cu\mathbf{L^4}H_2]^{4+}$, one must compare the deprotonation constants of these complexes with the corresponding deprotonation constants of $[Cu\mathbf{L^1}]^{4+}$ and $[Cu\mathbf{L^2}]^{4+}$ (Tables S2 and S3). For $[Cu\mathbf{L^3}H_2]^{4+}$, the two first deprotonation constants (pK_1 = 5.65 and pK_2 = 4.93) compare with the deprotonation of the $[Cu\mathbf{L^1}]^{4+}$ amide functions (pK_1 = 6.5 and pK_1 = 4.95), while the third and fourth deprotonation constants (pK_3 = 7.17 and pK_4 = 9.21) compare with the deprotonation of $\mathbf{L^1}$ amine functions (pKa_1 = 7.00 and pKa_2 = 9.19). One should also note that the species $[Cu\mathbf{L^3}H_2]^{4+}$ and $[Cu\mathbf{L^3}H]^{3+}$ are minor species, as already observed for the analogous complexes $[Cu\mathbf{L^1}]^{2+}$ and $[Cu\mathbf{L^1}H_{-1}]^{+}$. Hence, one can propose the following sequence: in $[Cu\mathbf{L^3}H_2]^{4+}$, copper complexation in one cavity causes the deprotonation of its amide groups, while the third and the fourth protons released come from the protonated second cavity (Figure 9a). For $[Cu\mathbf{L^4}H_2]^{4+}$, the same type of comparison allows the proposal of a different protonation sequence. The first deprotonation constant {pK_1 $[(Cu\mathbf{L^4}H_2)^{4+}]$ = 6.1} compares with the depro-

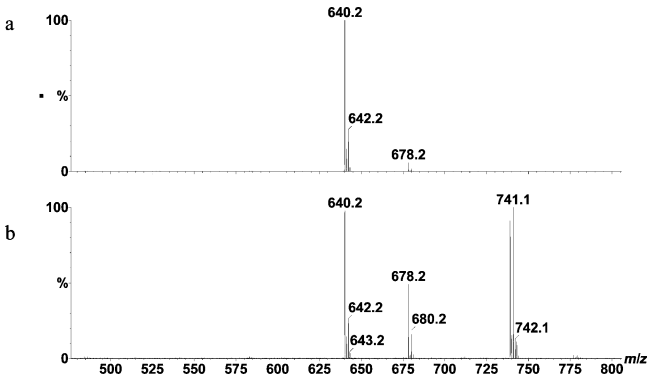

Figure 7. ESI-MS spectra of the {Cu–$\mathbf{L^3}$} solutions at pH 8.0, (a) R = [L]/[Cu^{2+}] = 1.08; (b) R = 0.61.

Table 5. ESI-MS spectrometry data for {Cu–$\mathbf{L^3}$} and {Cu–$\mathbf{L^4}$} solutions at different [L]/[M] ratios at pH 8.

Solution	Ratio [L]/[M]	*m/z*	Relative Intensity [%]	Elemental composition	Formula
Cu–$\mathbf{L^3}$	1.59	678.2	100	$C_{30}H_{40}N_8O_4CuK$	$[Cu\mathbf{L^3}H_{-2}K]^{+}$
		617.3	90	$C_{30}H_{42}N_8O_4K$	$\mathbf{L^3}K^{+}$
	1.08	678.2	10	$C_{30}H_{40}N_8O_4CuK$	$[Cu\mathbf{L^3}H_{-2}K]^{+}$
		640.2	100	$C_{30}H_{41}N_8O_4Cu$	$[Cu\mathbf{L^3}H_{-1}]^{+}$
	0.61	739.1	100	$C_{30}H_{38}N_8O_4Cu_2K$	$[Cu_2\mathbf{L^3}H_{-4}K]^{+}$
		678.2	50	$C_{30}H_{40}N_8O_4CuK$	$[Cu\mathbf{L^3}H_{-2}K]^{+}$
		640.2	100	$C_{30}H_{41}N_8O_4Cu$	$[Cu\mathbf{L^3}H_{-1}]^{+}$
Cu–$\mathbf{L^4}$	1.53	706.2	80	$C_{32}H_{44}N_8O_4CuK$	$[Cu\mathbf{L^4}H_{-2}K]^{+}$
		668.3	80	$C_{32}H_{45}N_8O_4Cu$	$[Cu\mathbf{L^4}H_{-1}]^{+}$
		645.3	100	$C_{32}H_{46}N_8O_4K$	$\mathbf{L^4}K^{+}$
		607.4	30	$C_{32}H_{47}N_8O_4$	$\mathbf{L^4}H^{+}$
	1.05	706.2	100	$C_{32}H_{44}N_8O_4CuK$	$[Cu\mathbf{L^4}H_{-2}K]^{+}$
		645.3	50	$C_{32}H_{46}N_8O_4K$	$\mathbf{L^4}K^{+}$
	0.55	767.2	100	$C_{32}H_{42}N_8O_4Cu_2K$	$[Cu_2\mathbf{L^4}H_{-2}K]^{+}$
		729.2	100	$C_{32}H_{43}N_8O_4Cu_2$	$[Cu_2\mathbf{L^4}H_{-2}]^{+}$
		706.2	80	$C_{32}H_{44}N_8O_4CuK$	$[Cu\mathbf{L^4}H_{-2}K]^{+}$
		668.3	20	$C_{32}H_{45}N_8O_4Cu$	$[Cu\mathbf{L^4}H_{-1}]^{+}$

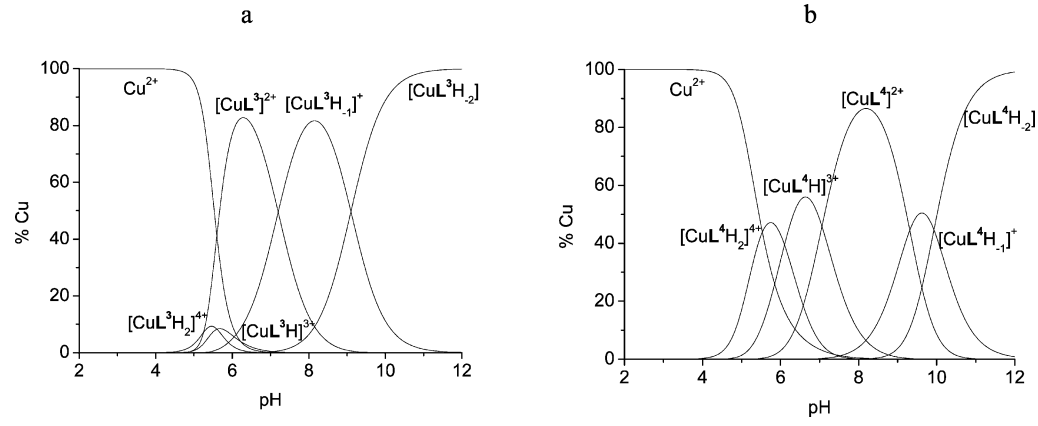

Figure 8. Species distribution diagrams for the Cu^{II} complexes with (a) $\mathbf{L^3}$ and (b) $\mathbf{L^4}$, $c_L = c_M = 2.50 \times 10^{-3}$ mol L^{-1}.

tonation of $\mathbf{L^2}H_2^{2+}$ [pKa_1 ($\mathbf{L^2}H_2^{2+}$) = 6.27], which indicates that the first proton released for $[Cu\mathbf{L^4}H_2]^{4+}$ comes from the free cavity. The second deprotonation constant {pK_2 $[(Cu\mathbf{L^4}H_2)^{4+}]$ = 7.06} compares with the deprotonation of $[Cu\mathbf{L^2}]^{2+}$ {pK_1 $[(Cu\mathbf{L^2})^{2+}]$ = 7.09}, which indicates that for $[Cu\mathbf{L^4}H_2]^{4+}$ the second proton released is from an amide function of the metallated cavity. The same analysis can be made for the third and the fourth deprotonation of $[Cu\mathbf{L^4}H_2]^{4+}$, which leads to the deprotonation of an amine function of the uncomplexed cavity {pK_3 $[(Cu\mathbf{L^4}H_2)^{4+}]$ = 9.31/pKa_2 ($\mathbf{L^2}H_2^{2+}$) = 9.41} followed by the deprotonation of the second amide function of the metallated cavity, respectively {pK_4 $[(Cu\mathbf{L^4}H_2)^{4+}]$ = 9.93/pK_2 $[(Cu\mathbf{L^2})^{2+}]$ = 10.0} (Figure 9b).

Table 6. Overall formation constants for $\mathbf{L^3}$ and $\mathbf{L^4}$.

log $\beta_{m\ell h}$	$\mathbf{L^3}$	$\mathbf{L^4}$
$Cu^{2+} + \mathbf{L} + 2H^+ \rightleftarrows [Cu\mathbf{L}H_2]^{4+}$	23.05(2)	22.90(1)
$Cu^{2+} + \mathbf{L} + H^+ \rightleftarrows [Cu\mathbf{L}H]^{3+}$	17.4(2)	16.8(1)
$Cu^{2+} + \mathbf{L} \rightleftarrows [Cu\mathbf{L}]^{2+}$	12.47(7)	9.74(1)
$Cu^{2+} + \mathbf{L} \rightleftarrows [Cu\mathbf{L}H_{-1}]^{+} + H^+$	5.3(3)	0.43(4)
$Cu^{2+} + \mathbf{L} \rightleftarrows [Cu\mathbf{L}H_{-2}] + 2H^+$	–3.91(8)	–9.5(1)
$2Cu^{2+} + \mathbf{L} \rightleftarrows [Cu_2\mathbf{L}]^{4+}$		13.87(4)
$2Cu^{2+} + \mathbf{L} \rightleftarrows [Cu_2\mathbf{L}H_{-2}]^{2+} + 2H^+$		0.2(2)
$2Cu^{2+} + \mathbf{L} \rightleftarrows [Cu_2\mathbf{L}H_{-3}]^{+} + 3H^+$		–9.8(2)
$2Cu^{2+} + \mathbf{L} \rightleftarrows [Cu_2\mathbf{L}H_{-4}] + 4H^+$		–20.0(2)

Incorporation of Two Cu^{II} Ions

In the presence of two equivalents of copper, precipitation occurs with $\mathbf{L^3}$, which prevents the determination of its complexation constants under these conditions. Hence, within the aim of developing ligands that allow the formation of soluble neutral copper complexes at physiological pH, $\mathbf{L^3}$ is no longer relevant. On the other hand, with $\mathbf{L^4}$, data analysis shows that the best fit of the titration curves involves the following species: $[Cu\mathbf{L^4}H_2]^{4+}$, $[Cu\mathbf{L^4}H]^{3+}$, $[Cu_2\mathbf{L^4}]^{4+}$, $[Cu_2\mathbf{L^4}H_{-2}]^{2+}$, $[Cu_2\mathbf{L^4}H_{-3}]^{+}$ and $[Cu_2\mathbf{L^4}H_{-4}]$. The ESI-MS spectra of these solutions (Figure 7) confirms the formation of a mixture of mono- (minor species) and dinuclear complexes. The overall complexation constants are gathered in Table 6, and the corresponding distribution curves are reported in Figure 10. It should be noted that below pH 5, mononuclear species are formed as the minor species. The log β value associated with the formation of $[Cu_2\mathbf{L^4}]^{4+}$ (log β_{210} = 13.87) is approximately twice that determined for $[Cu\mathbf{L^2}]^{2+}$ (log β_{110} = 6.89, Table 2) which suggests that in $[Cu_2\mathbf{L^4}]^{4+}$, as in $[Cu\mathbf{L^2}]^{2+}$, only the amine groups contribute significantly to metal coordination. In further steps, as the pH is increased, $[Cu_2\mathbf{L^4}]^{4+}$ is deprotonated. On the basis of these results, the successive deprotonation constants of $[Cu_2\mathbf{L^4}]^{4+}$ can be calculated (Table S3). The corresponding values indicate that for $[Cu_2\mathbf{L^4}]^{4+}$, the first value {pK $[(Cu_2\mathbf{L^4})^{4+}]$ = 13.67 Table 7} is approximately twice that calculated for the mononuclear homo-

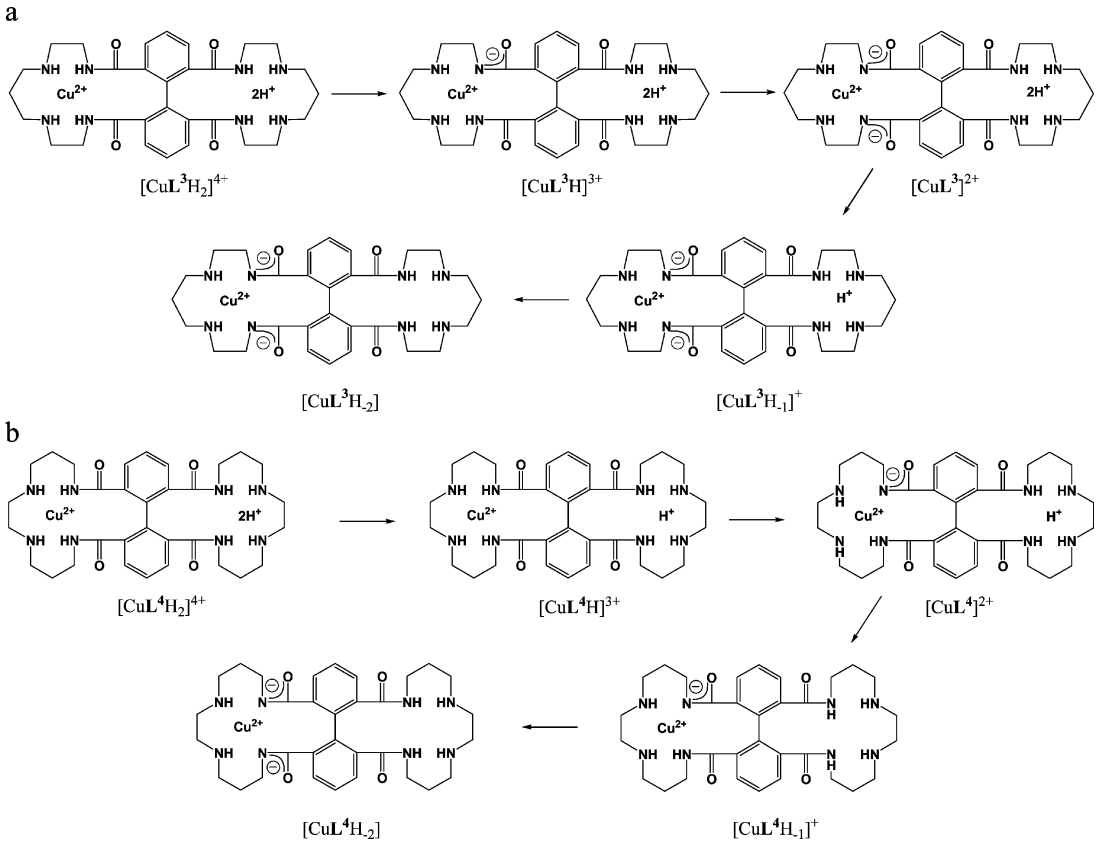

Figure 9. Deprotonation sequence suggested for: (a) $[Cu\mathbf{L^3}H_2]^{4+}$ and (b) $[Cu\mathbf{L^4}H_2]^{4+}$.

logue $[CuL^2]^{2+}$ (pK $[CuL^2]^{2+}$ = 7.09, Table 7). This means that in this step, two protons are released from $[Cu_2L^4]^{4+}$ to form $[Cu_2L^4H_{-2}]^{2+}$. In fact, in that case, the deprotonation constants associated with the two mono-deprotonation steps of $[Cu_2L^4]^{4+}$ are too close to be individually determined, and the value pK = 13.67 corresponds to the sum of these individual constants. Finally, at pH 7.4 for [L] = [M]/2 = 2.5×10^{-3} mol L^{-1}, the pCu value for L^4 is 3.87, which is similar to that determined previously for the analogous monomacrocycle L^2.

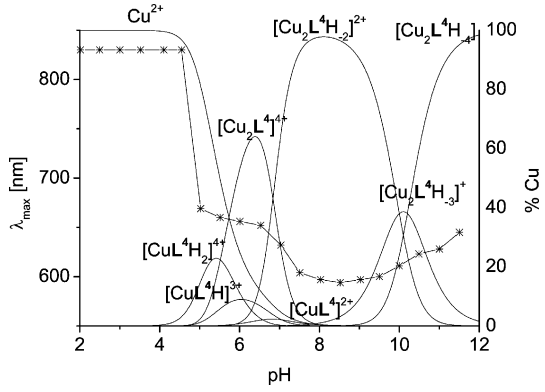

Figure 10. Species distribution diagram for the Cu^{II} complexes with L^4, $c_L = 2.50\times10^{-3}$ mol L^{-1}, $c_M = 1.25\times10^{-3}$ mol L^{-1}.

Table 7. Stepwise formation constants for the deprotonated species of $[Cu_2L^4]^{4+}$ and $[CuL^2]^{2+}$.

	pK
$[Cu_2L^4]^{4+} \rightleftarrows [Cu_2L^4H_{-2}]^{2+} + 2H^+$	13.67
$[Cu_2L^4H_{-2}]^{2+} \rightleftarrows [Cu_2L^4H_{-3}]^{+} + H^+$	10.0
$[Cu_2L^4H_{-3}]^{+} \rightleftarrows [Cu_2L^4H_{-4}] + H^+$	10.2
$[CuL^2]^{2+} \rightleftarrows [CuL^2H_{-1}]^{+} + H^+$	7.09
$[CuL^2H_{-1}]^{+} \rightleftarrows [CuL^2H_{-2}] + H^+$	10.0

In order to characterize the coordination sphere of copper in these complexes, the complexation process was followed by UV/Vis spectroscopy. For this study, L^4 was used as the hydrochloride salt. In the pH range 5–10, a blueshift of the signal is observed between 660 and 600 nm (Figure 10). This shift is similar to that previously described for L^2. Between pH 5 and 7, $[Cu_2L^4]^{4+}$, which is the major species, exhibits a broad band centred at 660 nm. This band can be correlated to that previously observed for $[CuL^2]^{2+}$, in which the metal is coordinated only by the amine functions of the ligand and by solvent molecules. As the pH is raised ($7 < pH < 10$), the band is blueshifted to 600 nm and is associated with the formation of $[Cu_2L^4H_{-2}]^{2+}$. By analogy with the corresponding $[CuL^2H_{-1}]^{+}$ complex, one can propose that in each macrocyclic cavity in $[Cu_2L^4H_{-2}]^{2+}$, the copper coordination sphere is composed of the two amine functions, one deprotonated amide function of the ligand and a solvent molecule. Finally above pH 10, the signal is redshifted from 600 to 650 nm. This process, which differs from that previously observed for $[CuL^2H_{-2}]$, is associated with the successive formation of the species $[Cu_2L^4H_{-3}]^{+}$ and $[Cu_2L^4H_{-4}]$. It is generally accepted that a redshift in the position of λ_{max} of a copper(II) complex in the visible region appears when the geometry around the metal changes from square-planar to octahedral.[26] The coordination sphere around each metal ion comprises two amine functions, two deprotonated amide functions and, probably, two chloride ions in the apical positions (since the ligand was used as the hydrochloride salt), which leads to an octahedral arrangement around the metal.

Solid-State Investigations

The complexes were obtained by addition of 2 equiv. $Cu(OAc)_2$ salt and 1 equiv. L^4 in methanol. Elemental analysis indicates that the synthesized complex corresponds to the formula $[Cu_2L^4(OAc)_4]$. Since attempts to obtain suitable crystals from $[Cu_2L^4(OAc)_4]$ failed, the environment around the metal was determined by IR and EPR spectroscopy.

The IR spectrum of $[Cu_2L^4(OAc)_4]$ exhibits three bands at 1630 [ν_{CO} (amide)], 1536 [ν_{as} (acetate)] and 1405 cm^{-1} [ν_s (acetate)] in the region for the carbonyl vibrations. These vibrations are close to those previously observed for $[CuL^2(OAc)_2]$, and the gap between these two absorption frequencies (Δ = 131 cm^{-1}) indicates that the coordination mode of the acetate counterions is similar to that in $[CuL^2(OAc)_2]$. Consequently one can propose that in $[Cu_2L^4(OAc)_4]$, the acetate ions are coordinated to the copper ions in a bidentate fashion (Figure 11).

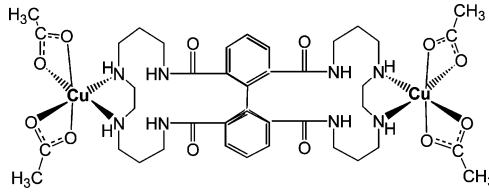

Figure 11. Structural hypothesis for $[Cu_2L^4(OAc)_4]$.

The EPR spectrum of $[Cu_2L^4(OAc)_4]$ can provide additional information about the respective positions of the two macrocyclic subunits. More precisely, it is expected that, according to the structure of the complex, if the two copper centres behave independently, the EPR signature of the complex (four lines in the parallel region of the spectrum) will be different from that expected if the two copper centers interact with each other (more than four lines in the parallel region of the spectrum).[28] The $[Cu_2L^4(OAc)_4]$ X-band EPR spectrum recorded in frozen methanol solution (150 K) exhibits a strong absorption at approximately 3200 G, which can be attributed to the allowed $\Delta M_S = 1$ transition (Figure 12). The hyperfine signal consists of four equidistant lines, which highlights that the two copper centres do not interact. In order to understand this behaviour and to correlate it to the overall structure of the complex, simulation of the EPR spectrum was undertaken with the X-Sophe software.[29,30] This simulation involves the building of the molecular Hamiltonian of the system, to obtain the spin parameters for the species $[Cu_2L^4(OAc)_4]$

and therefore to obtain structural information on the complex (distance between the two metal centres and respective orientation of the two macrocyclic subunits). For that, the spin Hamiltonian of a dinuclear complex is taken as:

$$H = \mu_B B g_A S_A + I_A A_A S_A + \mu_B B g_B S_B + I_B A_B S_B + J_{AB} S_A S_B + S_A D S_B$$

where μ_B is the Bohr magneton, g_A, g_B, A_A, and A_B correspond to the individual site g and A tensors, S_A and S_B are the spins on the two copper centres ($S_A = S_B = 1/2$), J_{AB} accounts for the isotropic exchange interaction and D is the zero-field-splitting tensor.[31,32] The J_{AB} and D parameters depend on the structural parameters defining the distance and orientation of the two metal centres (r_{AB}, τ, η and ζ) in the bis(dioxo) macrocyclic complex (Scheme S1). The spin Hamiltonian parameters of this complex are computed according to Comba's procedure[26] on the basis of the known parameters of the relevant mononuclear complex [Cu$\mathbf{L^2}$(OAc)$_2$] and on the estimation of the input values for D, the zero-field-splitting parameter, and r_{AB}, the metal–metal distance. In a first approximation, the orientation of the two macrocyclic subunits is assumed to be identical in the complex and in the ligand, i.e. more or less perpendicular.[27] Under these circumstances, the complex is centrosymmetric, which implies that the term D is nil.[33] In a second approximation, the r_{AB} distance between the two copper centres in the species [Cu$_2\mathbf{L^4}$(OAc)$_4$] is assumed to be twice the distance measured between the metal ion and the middle of the phenyl–phenyl distance (7 Å) in [Cu$\mathbf{L^2}$(OAc)$_2$].

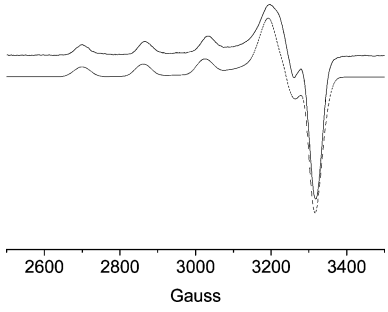

Figure 12. Experimental and simulated (dotted line) EPR spectra of [Cu$_2\mathbf{L^4}$(OAc)$_4$] in frozen methanol solution at 150 K.

After optimization, the resulting computed spectrum gives an acceptable fit with the experimental data (Figure 12 dotted lines), and the simulated EPR parameters are presented in Table 8. The computed values of $g_\perp$, $g_\parallel$ and $A_\parallel$ values for [Cu$_2\mathbf{L^4}$(OAc)$_4$] are similar to those for [Cu$\mathbf{L^2}$(OAc)$_2$]. The computed Cu–Cu distance obtained from the simulation is 8.9 Å, the angles (τ = 90°, η = 0° and ζ = 56°), which characterize the orientation of the two macrocyclic moieties, favour an orthogonal orientation of the cavities. These data are in close agreement with the structural features of $\mathbf{L^4}$[27] (distance between the centroids of each cavity = 7.36 Å and τ = 82°); this is not surprising since, if the two cavities behave independently, a difference between the shape of the ligand and the complex is not necessarily expected. Besides these geometrical considerations, the J_{AB} value can be obtained by simulation of the spectrum, and its optimized value (-12×10^{-4} cm^{-1}) confirms that the magnetic interaction is very weak in [Cu$_2\mathbf{L^4}$(OAc)$_4$]. This is the consequence of the orthogonal orientation of the magnetic copper orbitals in the dinuclear complex, which means that, in [Cu$_2\mathbf{L^4}$(OAc)$_4$], the two macrocyclic moieties are practically magnetically independent.

Table 8. Simulated EPR parameters for [Cu$_2\mathbf{L^4}$(OAc)$_4$].

$g_\perp$	2.052
$g_{//}$	2.265
$A_\perp$ (10^4 cm^{-1})	19.2
$A_\parallel$ (10^4 cm^{-1})	168.5
τ	90
η	0
ζ	56
r_{AB} [Å]	8.9
J (10^4 cm^{-1})	–12

Conclusions

The coordination constants of the Cu^{2+} complexes formed by the ligands $\mathbf{L^1}$–$\mathbf{L^4}$ in aqueous solution in the pH range 2–12 have been calculated, and the coordination numbers and geometries of the complexes have been established. Two complexation mechanisms have been identified according to the design of the ligands. With ligands $\mathbf{L^2}$ and $\mathbf{L^4}$ (for which the amino and the amido nitrogen atoms are separated by a chain of three carbon atoms), the complexation reaction above pH 11 involves three steps and forms the neutral copper complexes [Cu$\mathbf{L^2}$H$_{-2}$] or [Cu$_2\mathbf{L^4}$H$_{-4}$]. With ligand $\mathbf{L^1}$ on the other hand, the neutral complex [Cu$\mathbf{L^1}$H$_{-2}$] is more stable and is obtained in one step from pH 7. This can be correlated to the fact that, in $\mathbf{L^1}$, the lengths of the carbon chains between the successive nitrogen atoms induces better ligand preorganization. This preorganization promotes, as soon as the two amino nitrogen atoms are coordinated, the deprotonation of the two amide groups and then their simultaneous coordination. $\mathbf{L^1}$ is then the more significant ligand of the study for obtaining the desired neutral copper complexes at about pH 7. Nevertheless, the calculation of the pCu values for the ligands seems to indicate that the biphenyl substituent induces steric constraints that make these ligands less efficient than recent ligands[3] developed for radiomedical applications.

Experimental Section

General Information: All solvents were HPLC grade. The metals salts were purchased from Aldrich. The other reagents were used with the highest quality commercially available without further purification.

Ligand Synthesis: The ligands $\mathbf{L^1}$–$\mathbf{L^4}$ have been synthesized according to a new methodology developed by Hodakova et al.[27] The synthesis of the ligands started with biphenyl carboxylic acids (Scheme 3). Biphenyl-2,2′-dicarboxylic and biphenyl-2,2′,6,6′-tetracarboxylic acid were transformed to their acid chlorides on reac-

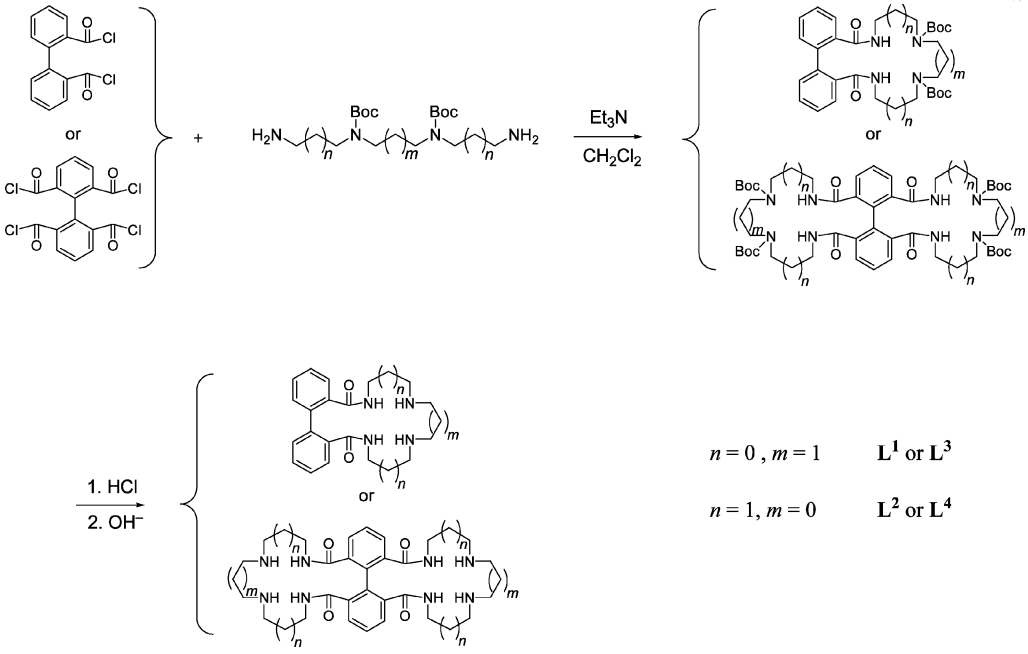

Scheme 3.

tion with thionyl chloride. Subsequently, under high-dilution conditions, cyclization of the biphenyl acid chloride with a selectively protected linear tetraamine [the central amine groups are protected by the *tert*-butoxycarbonyl (Boc) group, while the terminal amine groups are unprotected[34]] gave the protected monomacrocycles or bismacrocycles. Upon final deprotection with HCl(g), the hydrochlorides of ligands **L¹**–**L⁴** were obtained in nearly quantitative yields. The hydrochlorides were further transformed into the free bases: the hydrochlorides (1.5 mmol) were dissolved in water (50 mL) and then extracted into CH_2Cl_2 (3 × 100 mL). The organic layers were dried with K_2CO_3. After solvent removal, the crude free bases **L¹**–**L⁴** were crystallized from toluene or from a toluene/methanol mixture. The detailed NMR, IR and mass spectra of **L¹**–**L⁴** are reported in the Supporting Information.

Complex Synthesis: The neutral ligands **L¹** and **L²** (6.5×10^{-5} mol) were dissolved in methanol (10 mL), and a methanol solution of copper(II) acetate (6.8×10^{-5} mol in 5 mL) was added dropwise to each ligand solution. The mixtures were stirred for 2 h at room temperature. The solutions were further concentrated, and addition of diethyl ether allowed the precipitation of the complexes. The solids were then collected by filtration and dried under vacuum. Their purity was determined by elemental analysis. The solids were further dissolved in methanol, and diffusion of a diethyl ether solution gave single crystals of [Cu**L¹**H$_{-2}$] and [Cu**L²**(OAc)$_2$].

[CuL¹H$_{-2}$]·3.1H$_2$O: Blue solid. Yield: 71%, 16.9 mg. IR (KBr): $\nu_{(C=O)}$ = 1537 cm^{-1}, $\nu_{(CONH)}$ = 1445 cm^{-1}. ESI-MS: for [CuLH$_{-1}$]$^+$ *m*/*z* (%) = 428.1 (100), for [CuLH$_{-2}$K]$^+$ *m*/*z* (%) = 466.1 (10), for [LH]$^+$ *m*/*z* (%) = 367 (10). $C_{21}H_{24}N_4O_2Cu\cdot$**3**.1$H_2O$ (483.3): calcd. C 52.14, H 6.25, N 11.59; found C 51.83, H 5.67, N 11.70.

[CuL²(OAc)$_2$]·H$_2$O: Blue solid. Yield: 64%, 15.8 mg. IR (KBr): $\nu_{(C=O)}$ = 1628 cm^{-1}, $\nu_{(CONH)}$ = 1579 cm^{-1}, $\nu_{(C=O,s)}$(OAc) = 1393 cm^{-1}, $\nu_{(C=O,as)}$(OAc) = 1522 cm^{-1}. ESI-MS: for [CuLH$_{-1}$]$^+$ *m*/*z* (%) = 441.8 (100), for [CuL(OAc)]$^+$ *m*/*z* (%) = 501.8 (90), for [LH]$^+$ *m*/*z* (%) = 381 (10). $C_{26}H_{34}N_4O_6Cu\cdot H_2O$ (579.5): calcd. C 53.84, H 6.21, N 9.66; found C 54.05, H 5.90, N 10.39.

The neutral ligand **L⁴** (6.5×10^{-5} mol) was dissolved in methanol (10 mL), and a methanol solution of copper(II) acetate (13.5×10^{-5} mol in 5 mL) was added dropwise. The solution was mixed for 2 h at room temperature and further concentrated, and the addition of diethyl ether allowed the precipitation of the complex. The solid was then collected by filtration and dried under vacuum. Its purity was controlled by elemental analysis.

[Cu$_2$L⁴(OAc)$_4$]·6H$_2$O: Yield: 78%, 30.7 mg. IR (KBr): $\nu_{(C=O)}$ = 1630 cm^{-1}, $\nu_{(CONH)}$ = 1561 cm^{-1}, $\nu_{(C=O,s)}$(OAc) = 1405 cm^{-1}, $\nu_{(C=O,as)}$(OAc) = 1536 cm^{-1}. ESI-MS: for [Cu$_2$LH$_{-2}$(OAc)]$^+$ *m*/*z* (%) = 789.3 (100), for [Cu$_2$LH$_{-3}$]$^+$ *m*/*z* (%) = 729.3 (10). $C_{40}H_{46}N_8O_{12}Cu_2\cdot 6H_2O$ (1077): calcd. C 44.57, H 6.50, N 10.40; found C 44.51, H 5.95, N 10.55.

Potentiometric Measurements: Potentiometric titrations were carried out with an automatic titrator composed of a microprocessor burette Metrohm Dosimat 665 (1 mL capacity) and a pHmeter Metrohm 713 connected to a computer. The combined Type "U" glass electrode Metrohm used had a very low alkaline error. The titration procedure was fully automated. All measurements were performed within a thermoregulated cell at 25.0 ± 0.1 °C under an argon stream to avoid the dissolution of carbon dioxide. All equilibrium measurements were carried out in 10.00 mL sample volumes with magnetic stirring. The ionic strength was adjusted to 1 with potassium nitrate. An acetate buffer at 0.01 mol L^{-1} (I = 1) was prepared, for which the pH value was determined before use with a HNO_3 solution at exactly 10^{-2} mol L^{-1} (Normadose). This buffer solution was used to calibrate the electrode. The electrode slope was verified by titration with a HNO_3 solution, and no correction was necessary in the pH range 2 at 12. The titrant, a carbonate-free KOH solution (Normadose), was standardized against a 0.05 M potassium hydrogen phthalate solution by pH-potentiometry and used to verify the HNO_3 solution. The ionic product of water was determined under these conditions (pK_w = 13.78) and used in the calculations. A stock solution of $Cu(NO_3)_2$ was prepared from analytical grade salts (Aldrich 99.9%). The concentration of the stock solution was determined by complexometric ti-

tration with standardized Na_2H_2EDTA solution in the presence of PAN indicator. Solutions of ligand (1×10^{-3} to 5×10^{-3} mol L^{-1}) were titrated with standardized KOH solution (0.1001 mol L^{-1}). For the complexation studies, several ligand/copper nitrate mixtures were used (ligand/metal ratio in the range 1–2 for **L^1**–**L^2** or 0.5–2 for **L^3**–**L^4** with a ligand concentration of 2.5×10^{-3}mol L^{-1} in the measurement cell). The protometric data were processed by using the PROTAF program[15] to obtain the best-fit chemical model and refined overall constants β_{mlh}.

$$m\mathrm{M} + l\mathrm{L} + h\mathrm{H} \rightleftharpoons \mathrm{M}_m\mathrm{L}_l\mathrm{H}_h\beta_{mlh} = \frac{[\mathrm{M_m L_l H_h}]}{[\mathrm{M}]^m[\mathrm{L}]^l[\mathrm{H}^+]^h}$$

The stepwise protonation constants ($K_{0\ell h}$) related to Equilibrium (1) and defined by Equation (2) were deduced from the refined ($\beta_{0\ell h}$) values by Relation (3).

$$\mathrm{LH}_{h-1}^{(h-1)+} + \mathrm{H}^+ \overset{K_{0lh}}{\rightleftharpoons} \mathrm{LH}_h^{h+} \quad (1)$$

$$K_{0lh} = \frac{[\mathrm{LH_h}^{h+}]}{[\mathrm{LH}_{h-1}^{(h-1)+}][\mathrm{H}^+]} \quad (2)$$

$$\beta_{0\ell h} = \prod_{i=1}^{h} K_{0lh} \quad (3)$$

For each titration, at least 150 points per neutralization curve was used, and the titrations were repeated until a satisfactory agreement was reached. A minimum of 10 curves were used for the determination of the protonation constants of **L^1**–**L^4**, while for the determination of the complexation constants, two curves were used for each [L]/[M] ratio (resulting in a minimum of 10 curves for each ligand). For **L^3**–**L^4**, the potentiometric data used for the determination of the complexation constants of the mononuclear complexes with Cu^{II} corresponded to the ratios $C_L/C_M > 1$. Under these conditions, the mass spectra of the corresponding solutions recorded in water at different pH values confirm the sole presence of the mononuclear complexes. The potentiometric data used for the determination of the complexation constants of the dinuclear complexes corresponded to the ratios $C_L/C_M < 1$. Under these conditions, the mass spectra of the corresponding solutions recorded in water at different pH values confirm the presence of mono- and dinuclear complexes.

In aqueous solutions, the visible spectra of the copper(II) complexes were recorded with a Shimadzu UV-2401-PC spectrophotometer equipped with a standard syringe shipper and a temperature-controlled TCC-240A cell holder. The experiments were monitored in the concentration range used for the pH titration; averages of 25 spectra were recorded in the pH range from 3 to 11.5. The overall stability constants of the ligands **L^1**–**L^2** ($\beta_{m\ell h}$) of the copper(II) complexes were calculated with the general computation program HYPERQUAD.[35]

The pCu values were calculated with the program HYSS,[35b] under the following conditions: pH 7.4, [L] = [M] = 5×10^{-3} mol L^{-1} for **L^1** and **L^2**, [L] = [M]/2 = 2.5×10^{-3} mol L^{-1} for **L^4**.

Spectroscopic Measurements: NMR spectra were measured on a Varian Unity 500 (^{1}H at 499.9 MHz, and ^{13}C at 125.7 MHz) by using tetramethylsilane as an internal standard. The assignment of the structure is based on characteristic chemical shifts, multiplicities and intensities of individual signals, and in some cases on homonuclear 2D-COSY and heteronuclear 2D-HMQC spectra. Values of the coupling constants J are given in Hz. IR spectra were recorded with an IR AVATAR 320 FTIR spectrophotometer as KBr pellets. The UV/Vis spectra in methanol or in the solid state were recorded on a Varian Cary 5000 spectrophotometer completed with internal diffuse reflectance accessories. Mass spectrometry: for the ligands **L^1**–**L^4**, mass spectra were recorded on a ZAB-EQ instrument (VG Analytical) by using the FAB (Xe, 8 kV) ionization technique and a thioglycerol-glycerol (3:1) mixture as a matrix. For the complexes, the experiments were performed with a Q-TOF mass spectrometer (Micromass, Manchester, UK) equipped with an electrospray ionization (ESI) source operated in the positive ion mode. The capillary voltage was set at 3500 V and the declustering potential at 60 V. In this hybrid instrument, ions were measured using an orthogonal acceleration time-of-flight (oa-TOF) mass analyzer. Nitrogen was used as the nebulizing gas at a pressure of 10 psi, the curtain gas (20 psi). Analyst software version 4.0 (MassLynx) was used for instrument control, data acquisition and data processing. Aqueous solutions were introduced into the ionization source at a flow rate of 5 mL/min using a syringe pump. EPR spectra were recorded with a Bruker ESP300e spectrometer (X-band) equipped with a Bruker E035M gaussmeter and an HP 5350B microwave frequency counter. Samples were prepared at a concentration of 5 mmol L^{-1} in methanol or water/glycerol (90:10) frozen solutions (150 K, Bruker ER4111VY variable-temperature unit). The best resolution was obtained at T = 150 K by using a modulation amplitude of 4.217 G, a time constant of 655.36 ms, a conventional time of 327.68 ms and a sweep time of 335.54 ms. The simulation of the EPR spectra was performed by using X-sophe software version 1.1.4 for Mandriva 2006 x86–64 developed by the Centre for Magnetic Resonance and the Department of Mathematics at the University of Queensland, Brisbane, Australia, for Bruker Biospin GmbH.[29]The software uses a linewidth model with an angular dependence of g and a Simplex optimisation method with the copper element in natural abundance {for (Cu**L^1**H$_{-2}$): linewidth in the parallel region 21.9×10^{-4} cm^{-1}, in the perpendicular region 39.6×10^{-4} cm^{-1}; for [Cu**L^2**(OAc)$_2$]: linewidth in the parallel region 22.4×10^{-4} cm^{-1}, in the perpendicular region 23.1×10^{-4} cm^{-1}; for [Cu$_2$**L^4**(OAc)$_4$]: linewidth in the parallel region 19.1×10^{-4} cm^{-1}, in the perpendicular region 16.8×10^{-4} cm^{-1}}.

Crystal Structure Determination: The crystal data were collected at 100 K with a Kappa CCD diffractometer by using monochromated Mo-K_α radiation (λ = 0.71073 Å). The structures were solved by direct methods. After refinement of the non-hydrogen atoms, difference-Fourier maps revealed maxima of the residual electron density close to positions expected for the hydrogen atoms. Hydrogen atoms were introduced as fixed contributors at calculated positions [C–H 0.95 Å, B(H) 1.3 Beqv.]. Final difference maps revealed no significant maxima. All calculations were performed with the Nonius OpenMoleN package.[36] Neutral atom scattering factor coefficients and anomalous dispersion coefficients were taken from a standard source. Crystal data and details of the structure determination for [Cu**L^1**H$_{-2}$] and [Cu**L^2**(OAc)$_2$] are given in Supporting Information (Table S1). CCDC-717581 ([Cu**L^1**H$_{-2}$]) and -717580 ([Cu**L^2**(OAc)$_2$]) contains the supplementary crystallographic data (excluding structure factors) for this paper. These data can be obtained free of charge from The Cambridge Crystallographic Data Centre via www.ccdc.cam.ac.uk/data_request/cif.

Supporting Information (see footnote on the first page of this article): The detailed NMR, IR and mass spectra of **L^1**–**L^4** are reported. Titrations curves for solutions of **L^1**–**L^4** (Figure S1), experimental and simulated EPR spectra of the **L^1**,**L^2**/Cu^{2+} systems (Figure S2), crystal data for [Cu**L^1**H$_{-2}$] and [Cu**L^2**(OAc)$_2$] (Table S1), successive deprotonation constants for [Cu**L^3**H$_2$]$^{4+}$ (Table S2) and for [Cu**L^4**H$_2$]$^{4+}$ (Table S3) and the definition of the structural pa-

rameters used in the spin Hamiltonian for the simulation of the EPR spectra of the dinuclear complexes (Scheme S1) are also given.

[1] I. Tabushi, Y. Tanigushi, H. Kato, *Tetrahedron Lett.* **1977**, *18*, 1049–1052.

[2] a) M. Kodama, E. Kimura, *J. Chem. Soc., Dalton Trans.* **1979**, 1783–1789; b) M. Kodama, E. Kimura, *J. Chem. Soc., Dalton Trans.* **1981**, 694–700; c) E. Kimura, A. Sakonaka, R. Machida, M. Kodama, *J. Am. Chem. Soc.* **1982**, *104*, 4255–4257; d) R. Machida, E. Kimura, M. Kodama, *Inorg. Chem.* **1983**, *22*, 2055–2061.

[3] P. Antunes, R. Delgado, M. G. B. Drew, V. Felix, H. Maecke, *Inorg. Chem.* **2007**, *46*, 3144–3153.

[4] R. J. Motekaitis, Y. Sun, A. E. Martell, M. Welch, *Can. J. Chem.* **1999**, *77*, 614–623.

[5] a) E. Kimura, *Tetrahedron* **1992**, *48*, 6175–6217; b) R. Machida, E. Kimura, M. Kodama, *Inorg. Chem.* **1983**, *22*, 2055–2061.

[6] a) P. A. Vigato, S. Tamburini, D. E. Fenton, *Coord. Chem. Rev.* **1990**, *106*, 25–170; b) C. T. Chen, K. S. Suslick, *Coord. Chem. Rev.* **1993**, *128*, 293–322.

[7] a) O. Kahn, Y. Pei, M. Verdaguer, J. P. Renard, J. Sletten, *J. Am. Chem. Soc.* **1988**, *110*, 782–789; b) K. Nakatani, J. Y. Carriat, Y. Journaux, O. Kahn, F. Lloret, J. P. Renard, Y. Pei, J. Sletten, M. Verdaguer, *J. Am. Chem. Soc.* **1989**, *111*, 5739–5748; c) L. Cronin, A. R. Mount, S. Parsons, N. Robertson, *J. Chem. Soc., Dalton Trans.* **1999**, 1925–1928; d) L. N. Zhu, N. Xu, W. Zhang, D. Z. Liao, K. Yoshimura, K. Mibu, Z. H. Jiang, S. P. Yan, P. Cheng, *Inorg. Chem.* **2007**, *46*, 1297–1304.

[8] a) A. Aurora, M. Boiocchi, G. Dacarro, F. Foti, C. Mangano, P. Pallavicini, S. Patroni, A. Taglietti, R. Zanoni, *Chem. Eur. J.* **2006**, *12*, 5535–5546; b) V. Amendola, L. Fabbrizzi, C. Mangano, P. Pallavicini, *Acc. Chem. Res.* **2001**, *34*, 488–493; V. Amendola, L. Fabbrizzi, C. Mangano, H. Miller, P. Pallavicini, A. Perotti, A. Taglietti, *Angew. Chem. Int. Ed.* **2002**, *41*, 2553–2556.

[9] L. Fabbrizzi, F. Foti, S. Patroni, P. Pallavicini, A. Taglietti, *Angew. Chem. Int. Ed.* **2004**, *43*, 5073–5077.

[10] T. M. Jones-Wilson, K. A. Deal, C. J. Anderson, D. W. Mc Carthy, Z. Kovacs, R. J. Motekaitis, A. D. Sherry, A. E. Martell, M. J. Welch, *Nucl. Med. Biol.* **1998**, *25*, 523–530.

[11] a) C. S. Cutler, M. Wuest, C. J. Anderson, D. E. Reichert, Y. Sun, A. E. Martell, M. J. Welch, *Nucl. Med. Biol.* **2000**, *27*, 375–380; b) X. Sun, J. Kim, A. E. Martell, M. J. Welch, C. J. Anderson, *Nucl. Med. Biol.* **2004**, *31*, 1051–1059.

[12] D. E. Reichert, J. S. Lewis, C. J. Anderson, *Coord. Chem. Rev.* **1999**, *184*, 3–66.

[13] a) S. V. Smith, *J. Inorg. Biochem.* **2004**, *98*, 1874–1901; b) T. J. Wadas, E. H. Wong, G. R. Weisman, C. J. Anderson, *Curr. Pharm. Des.* **2007**, *13*, 3–16; c) P. J. Blower, J. S. Lewis, J. Zweit, *Nucl. Med. Biol.* **1996**, *23*, 957–980.

[14] a) C. A. Boswell, C. A. S. Regino, K. E. Baidoo, K. J. Wong, D. E. Milenic, J. A. Kelley, C. C. Lai, M. W. Brechbiel, *Bioorg. Med. Chem. Lett.* **2009**, *17*, 548–552; b) S. Liu, *Adv. Drug Delivery Rev.* **2008**, *60*, 1347–1370; c) C. T. Yang, Y. S. Kim, J. Wang, L. Wang, J. Shi, Z. B. Li, X. Chen, M. Fan, J. J. Li, S. Liu, *Bioconjugate Chem.* **2008**, *19*, 2008–2022; d) J. E. Sprague, Y. Peng, A. L. Fiamengo, K. S. Woodin, E. A. Southwick, G. R. Weisman, E. H. Wong, J. A. Golen, A. L. Rheingold, C. J. Anderson, *J. Med. Chem.* **2007**, *50*, 2527–2535; e) H. S. Chong, S. Lim, K. E. Baidoo, D. E. Milenic, X. Ma, F. Jia, H. A. Song, M. W. Brechbiel, M. R. Lewis, *Bioorg. Med. Chem. Lett.* **2008**, *18*, 5792–5795.

[15] a) R. Fournaise, C. Petitfaux, *Talanta* **1987**, *34*, 385–395; b) R. Fournaise, C. Petitfaux, *Analysis* **1990**, *18*, 242–249.

[16] L. Fabbrizzi, F. Forlini, A. Perotti, B. Seghi, *Inorg. Chem.* **1984**, *23*, 807–813.

[17] a) M. Chadim, P. Diaz, E. Garcia-Espana, J. Hodacova, P. C. Junk, J. Latorre, J. M. Llinares, C. Soriano, J. Zavada, *New J. Chem.* **2003**, *27*, 1132–1139; b) P. Arranz, A. Bencini, A. Bianchi, P. Diaz, E. Garcia-Espana, C. Giorgi, S. V. Luis, M. Querol, B. Valtancoli, *J. Chem. Soc. Perkin Trans. 2* **2001**, 1765–1770.

[18] D. Chen, Y. Sun, A. E. Martell, M. J. Welch, *Inorg. Chim. Acta* **2002**, *335*, 119–124.

[19] a) M. Soibinet, I. Déchamps-Olivier, E. Guillon, J. P. Barbier, M. Aplincourt, F. Chuburu, M. Le Baccon, H. Handel, *Eur. J. Inorg. Chem.* **2003**, 1984–1994; b) S. Develay, R. Tripier, M. Le Baccon, V. Patinec, G. Serratrice, H. Handel, *Dalton Trans.* **2005**, 3016–3024.

[20] B. J. Hathaway, *J. Chem. Soc., Dalton Trans.* **1972**, 1196–1199.

[21] U. Sagakuchi, A. W. Addison, *J. Chem. Soc., Dalton Trans.* **1979**, 600–608.

[22] E. Kimura, *J. Coord. Chem.* **1986**, *15*, 1–28.

[23] G. B. Deacon, R. J. Phillips, *Coord. Chem. Rev.* **1980**, *33*, 227–250.

[24] V. Robert, G. Lemercier, *J. Am. Chem. Soc.* **2006**, *128*, 1183–1187.

[25] Y. Dong, G. A. Lawrence, L. F. Lindoy, P. Turner, *Dalton Trans.* **2003**, 1567–1576.

[26] a) E. Prenesti, P. G. Daniele, M. Prencipe, G. Ostacoli, *Polyhedron* **1999**, *18*, 3233–3241; b) E. Prenesti, P. G. Daniele, S. Berto, S. Toso, *Polyhedron* **2006**, *25*, 2815–2823.

[27] S. Koscova, M. Budesinsky, B. Klepetarova, Peter C. Junk, J. Hodacova, manuscript in preparation.

[28] a) E. F. Hasty, L. J. Wilson, D. N. Hendrickson, *Inorg. Chem.* **1978**, *17*, 1834–1841; b) C. He, S. J. Lippard, *Inorg. Chem.* **2000**, *39*, 5225–5231; c) R. P. Houser, V. G. Young, W. B. Tolman, *J. Am. Chem. Soc.* **1996**, *118*, 2101–2102; d) R. Gupta, Z. H. Zhang, D. Powell, M. P. Hendrich, A. S. Borovik, *Inorg. Chem.* **2002**, *41*, 5100–5106; e) S. P. Foxon, G. R. Torres, O. Walter, J. Z. Pedersen, H. Toftlund, M. Hüber, K. Falk, W. Haase, J. Cano, F. Lloret, M. Julve, S. Schindler, *Eur. J. Inorg. Chem.* **2004**, 335–343.

[29] M. Griffin, A. Muys, C. Noble, D. Wang, C. Eldershaw, K. E. Gates, K. Burrage, G. R. Hanson, *Mol. Phys. Rep.* **1999**, *26*, 60–84.

[30] G. R. Hanson, K. E. Gates, C. J. Noble, M. Griffin, A. Mitchell, S. Benson, *J. Inorg. Biochem.* **2004**, *98*, 903–916.

[31] P. Comba, Y. D. Lampeka, A. I. Prikhod′ko, G. Rajaraman, *Inorg. Chem.* **2006**, *45*, 3632–3638.

[32] T. D. Smith, J. R. Pilbrow, *Coord. Chem. Rev.* **1974**, *13*, 173–278.

[33] J. R. Pilbrow, *Transition Ion Electron Paramagnetic Resonance*, Oxford University Press, New York, **1991**, p. 334.

[34] S. Koscova, M. Budesinsky, J. Hodacova, *Collect. Czech. Chem. Commun.* **2003**, *68*, 744–750.

[35] a) P. Gans, A. Sabatini, A. Vacca, *Talanta* **1996**, *43*, 1739–1757; b) L. Alderighi, P. Gans, A. Ienco, D. Peters, A. Sabatini, A. Vacca, *Coord. Chem. Rev.* **1999**, *184*, 311–318.

[36] OpenMoleN, *Interactive Structure Solutions*, Nonius B. V. Delft, The Netherlands, **1997**.

Received: January 30, 2009
Published Online: June 5, 2009

